Letter

Enhancement of Josephson Critical Currents in Ferromagnetic $Co_{40}Fe_{40}B_{20}$ by Thermal Annealing

Sachio Komori,[1,2,†] Juliet E. Thompson,[1,†] Guang Yang,[1,3] Graham Kimbell,[1] Nadia Stelmashenko,[1] Mark G. Blamire,[1] and Jason W. A. Robinson[1,*]

[1] *Department of Materials Science & Metallurgy, University of Cambridge, 27 Charles Babbage Road, Cambridge CB3 0FS, United Kingdom*

[2] *Department of Physics, Nagoya University, Furo-cho, Chikusa-ku, Nagoya 464-8602, Japan*

[3] *Fert Beijing Institute, MIIT Key Laboratory of Spintronics, School of Integrated Circuit Science and Engineering, Beihang University, Beijing, 100191, China*

(Received 30 March 2021; revised 30 August 2021; accepted 11 January 2022; published 15 February 2022)

The electrical and structural properties of $Co_{40}Fe_{40}B_{20}$ (Co-Fe-B) are tunable by thermal annealing. This is key to the optimization of Co-Fe-B-based spintronic devices, where the advantageously low magnetic coercivity, high spin polarization, and controllable magnetocrystalline anisotropy are utilized. Here, we report Nb/Co-Fe-B/Nb Josephson devices and demonstrate an enhancement of the critical current by up to 700% following thermal annealing due to increased structural ordering of the Co-Fe-B. The results demonstrate that Co-Fe-B is a promising material for superconducting quantum spintronic devices.

DOI: 10.1103/PhysRevApplied.17.L021002

Following the discovery of giant magnetoresistance [1,2] and the development of spin valves [3,4], $Co_{40}Fe_{40}B_{20}$ (Co-Fe-B) was identified as an alternative magnetic material to those that had previously been employed, particularly due to its low magnetic anisotropy and low switching energy [5,6]. In Co-Fe-B spintronic devices, the magnetoresistance can be optimized through a thermal annealing [7]. Specifically, for Co-Fe-B/MgO/Co-Fe-B magnetic tunnel junctions, thermal-annealing treatment leads to high tunneling magnetoresistance, exceeding 600% at room temperature [8]; neither Co-Fe-B nor Co-Fe as-grown devices display comparable efficiencies. Studies of diffusive (i.e., without a tunnel junction) Co-Fe-B spin valves have also demonstrated larger giant magnetoresistance effects following annealing treatment [9].

Although the advantageous properties of Co-Fe-B-based spintronic devices and their controllability through annealing have been well recognized in the field of spintronics, there has been only one other report on superconducting devices with Co-Fe-B [10]. This may be due to the strong magnetic exchange energy and the high electrical resistivity of Co-Fe-B [11], which should strongly quench the superconducting proximity effect, making it challenging to investigate the coupling of superconductivity and magnetism. However, the superconducting proximity effect in Co-Fe-B could enable energy-efficient and fast superconducting (Josephson) devices because the low coercivity of Co-Fe-B reduces the energy required for writing operation and the large resistivity reduces the switching time $\tau = \Phi_0/2\pi I_c R_N$ [12–14], where Φ_0 is the magnetic flux quantum, I_c is the Josephson critical current, and R_N is the normal state resistance.

Here, we report Nb/Co-Fe-B/Nb Josephson devices with thin (<5 nm) Co-Fe-B barriers and investigate the effect of thermal annealing on the critical current. From measurement of the Josephson critical currents versus Co-Fe-B barrier thickness, we determine a superconducting coherence length in Co-Fe-B of approximately 1 nm. Annealing the devices at 400 °C for 30 min in vacuum results in the increase in the critical current by as much as 700% for a Co-Fe-B thickness of 4 nm. We associate this enhancement of the Josephson current with an increase in the electron mean-free-path length (i.e., reduced charge and spin-flip scattering) in Co-Fe-B along with improved transparency at the Nb/Co-Fe-B interfaces.

Nb(300 nm)/Co-Fe-B(d_F)/Nb(300 nm) trilayers are fabricated on 5×5 mm^2 quartz substrates by dc magnetron sputtering in an ultrahigh-vacuum chamber with a base pressure better than 10^{-6} Pa. The sputtering targets ($Co_{40}Fe_{40}B_{20}$, Nb) are presputtered for 20 min to clean their surfaces. The films are grown in Ar at a pressure of 1.5 Pa at room temperature. Multiple quartz substrates are placed on a rotating circular table that pass below a series of stationary magnetrons. A series of stacks are prepared with different Co-Fe-B thicknesses

*jjr33@cam.ac.uk

†These authors contributed equally to this work.

($d_F = 1.5$–4.5 nm) between 300-nm-thick layers of Nb in a single deposition. Layer thicknesses are controlled by adjusting the angular speed of the rotating table.

Current-perpendicular-to-plane Nb(300 nm)/Co-Fe-B (d_F)/Nb(300 nm) nanopillar devices with square cross-section areas of about $A = 500 \times 500$ nm^2 are fabricated using a focused beam of Ga ions as described elsewhere [15]. A pulse-tube cryogen-free measurement system (Cryogenic Ltd) is used to cool the devices down to 1.6 K. Current-voltage $I(V)$ characteristics of the nanopillars are measured in a four-point configuration using the differential conductance mode of a Keithley 6221 ac-current source and a 2182 A nanovoltmeter. The Josephson critical current and normal state resistance of each device are determined by fitting the $I(V)$ characteristics to the resistively shunted junction model $V = R_N(I^2 - I_c{}^2)^{0.5}$. Since the coherence length in a ferromagnet is $\xi_F = (\hbar D_F/2\pi E_{\mathrm{ex}})^{0.5}$ in the diffusive limit [16] and I_c is proportional to $\exp(-d_F/\xi_F)$ [16], I_c enhancement can be realized by increasing the diffusion constant (D_F) or decreasing the magnetic exchange energy (E_{ex}) of the ferromagnet. Electrical measurements are performed on nanopillars both before and after thermal annealing. Thermal annealing is performed at 400 °C for 30 min in vacuum (10^{-5} Pa)—the typical postanneal condition [8,17] to promote crystallization. No magnetic field is applied during annealing. Annealed Co-Fe-B has lower resistivity than amorphous Co-Fe-B deposited at room temperature [18]. Although electrical properties of our Co-Fe-B films become increasingly metallic with annealing [see Fig. S2(b) within the Supplemental Material [19]], we can not detect x-ray diffraction peaks from the Co-Fe-B layer, which is likely due to small grain size of Co-Fe-B in the absence of a buffer layer (e.g., MgO [20]) that can promote crystallization with large grain size.

A typical Fraunhofer pattern, the critical current density J_c versus in-plane magnetic field H, for a Nb(300 nm)/Co-Fe-B(3.5 nm)/Nb(300 nm) nanopillar at 1.6 K before (solid curves) and after (dashed curves) thermal annealing is shown in Fig. 1(a) (see Fig. S1 within the Supplemental Material [19] for all the Fraunhofer patterns recorded in this study). $J_c(H)$ is hysteretic and the maximum values of I_c are obtained at nonzero applied fields ($\mu_0 H = \delta$) due to the intrinsic barrier magnetization [21,22]. In Fig. 1(b), we plot δ at 1.6 K versus d_F, which shows a linear increase in δ with d_F. By fitting δ versus d_F to $\delta = M_s(d_F - d_{\mathrm{dead}})/(2\lambda + d_F)$ [21], we obtain a volume saturation magnetization of $M_s = (643 \pm 21)$ emu cm^{-3}, and a magnetically dead layer thickness at each Nb/Co-Fe-B interface of $d_{\mathrm{dead}} = (0.33 \pm 0.09)$ nm, which is slightly thinner than those at Nb/Co ($d_{\mathrm{dead}} = 0.4$ nm) and Nb/Fe ($d_{\mathrm{dead}} = 0.55$ nm) interfaces [23] and consistent with the magnetization measurements of unpatterned Nb(30 nm)/Co-Fe-B(2–10 nm)/Nb(30 nm) samples [see Fig. S4(b) within the Supplemental Material [19]]. Here, $\lambda = 110$ nm [24,25] is an estimate of the London penetration depth of polycrystalline Nb. M_s obtained here is smaller than the maximum bulk

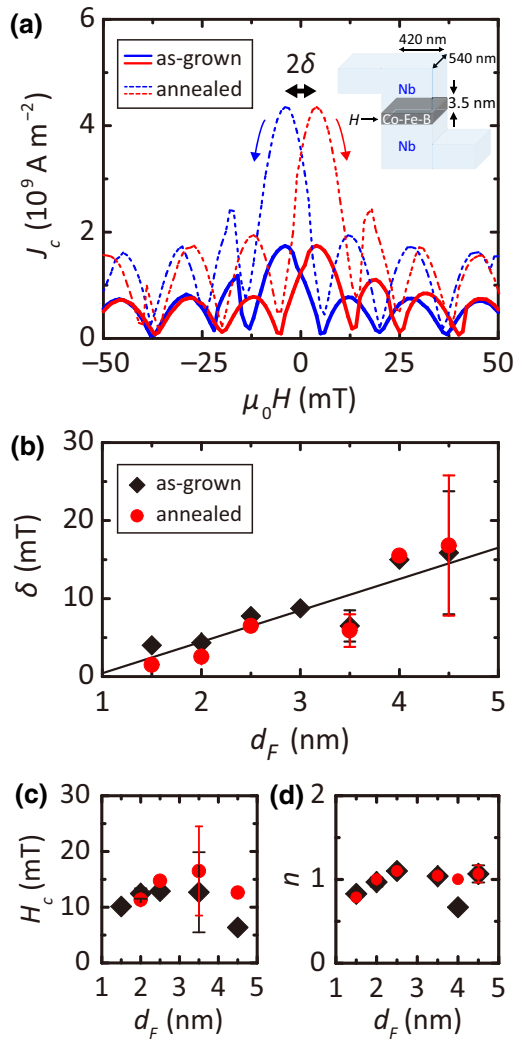

FIG. 1. (a) $J_c(H)$ pattern for a Nb(300 nm)/Co-Fe-B(3.5 nm)/Nb(300 nm) nanopillar before (solid lines) and after (dashed lines) thermal annealing at 400 °C for 30 min. The red (solid and dashed) line shows J_c with increasing H and the blue (solid and dashed) line shows J_c with decreasing H. The inset shows a schematic diagram of a nanopillar. (b) In-plane magnetic hysteresis (δ) for Nb(300 nm)/Co-Fe-B(d_F)/Nb(300 nm) nanopillars before (black diamonds) and after (red circles) thermal annealing. The vertical error bars represent the statistical scatter of δ for multiple nanopillars on the same circuit. The black line is a least-squares regression-line fit for the nanopillars before thermal annealing, giving a volume saturation magnetization of (643 ± 21) emu cm^{-3} and a magnetically dead layer thickness at each Nb/Co-Fe-B interface of (0.33 ± 0.09) nm. (c) An estimate of the coercive field (H_c) of the nanopillars versus d_F and (d) the magnetic field periodicity (n) of $I_c(H)$ versus d_F before (black diamonds) and after (red circles) thermal annealing. All data at 1.6 K.

magnetization of 1300 emu cm^{-3} [11,26], implying a reduced magnetization in thin (<5 nm) Co-Fe-B and, possibly, partial oxidation or Ga implantation in nanopillars. For $d_F = 4.5$ nm, the magnetization of Co-Fe-B switches at $\mu_0 H_c < M_s(d_F - d_{\text{dead}})/(2\lambda + d_F)$ and hence the maximum in J_c occurs at $\delta \approx \mu_0 H_c$, resulting in a spread in δ due to variations in H_c. The relatively large deviations of δ for $d_F = 3.5$ and 4.5 nm from the linear fit are likely due to the variation in M and potential magnetic inhomogeneity [21] in the nanopillars at low fields. A clear change in δ is not observed following thermal annealing, suggesting that the magnetization of Co-Fe-B in nanopillars is unaffected by annealing, consistent with our magnetization measurements of unpatterned films [see Fig. S2(a) within the Supplemental Material [19]]. We estimate H_c of the nanopillars from H where the hysteresis of the $I_c(H)$ curves closes to δ (see Fig. S5 within the Supplemental Material [19]). For the d_F range investigated in this study, $\mu_0 H_c \approx 10$ mT [see Fig. 1(c)], consistent with the fact that $\delta \approx \mu_0 H_c$ at $d_F = 4.5$ nm. In Fig. 1(d), we plot the normalized magnetic field periodicity (n) of $I_c(H)$ versus d_F, where n is determined from sinc $(n\Phi/\Phi_0)$ with $\Phi = \mu_0 HL(2\lambda + d_F)$ and L is the length of the junction perpendicular to the applied magnetic field. For the d_F range investigated, $n \approx 1$, indicating homogeneous supercurrents across the device areas and the absence of an anomalous higher (second) harmonic current-phase relationship, which has been reported for Josephson junctions with ferromagnetic barriers at a 0–π phase transition [23,27,28].

In Fig. 2(a), we plot the total specific resistance of the nanopillars (AR_N) versus d_F at 1.6 K before and after thermal annealing. From a least-squares regression-line fit ($AR_N = \rho_F \times d_F + 2AR_{\text{Nb/Co-Fe-B}}$), we estimate an as-grown Co-Fe-B resistivity of $\rho_F = (88 \pm 46)$ $\mu\Omega$ cm, which is higher than the resistivity of a $Co_{60}Fe_{40}$ polycrystalline ferromagnetic alloy ($\rho \approx 15$ $\mu\Omega$ cm at 10 K [29]). We also estimate the specific resistances of the two Nb/Co-Fe-B interfaces as $2AR_{\text{Nb/Co-Fe-B}} = (4.4 \pm 1.4)\, f\,\Omega$ m^2. The effective electron mean free path in as-grown Co-Fe-B is $l = 3\pi^2\hbar/k_F{}^2 e^2 \rho_F = (1.8 \pm 0.9)$ nm, where $\hbar$ is the Planck constant divided by 2π, $k_F = 0.104$ nm^{-1} [30] is the Fermi wave number in the majority band of Co-Fe-B, and e is the elementary charge. We observe a decrease in AR_N for all the devices following thermal annealing, suggesting a decrease in ρ_F (and increase in the electron mean-free-path length) as a result of increased structural order. The increased degree of scatter in AR_N versus d_F for the nanopillars after thermal annealing is likely due to the variation of the resistance of Co-Fe-B and Nb/Co-Fe-B interfaces induced by annealing. Such a variation is likely due to the stochastic nature of nucleation of structural changes affecting the electronic band structure and the resistivity at the Nb/Co-Fe-B interfaces. We estimate $2AR_{\text{Nb/Co-Fe-B}} = (2.1 \pm 1.7)$ $f\,\Omega$ m^2 for the nanopillars

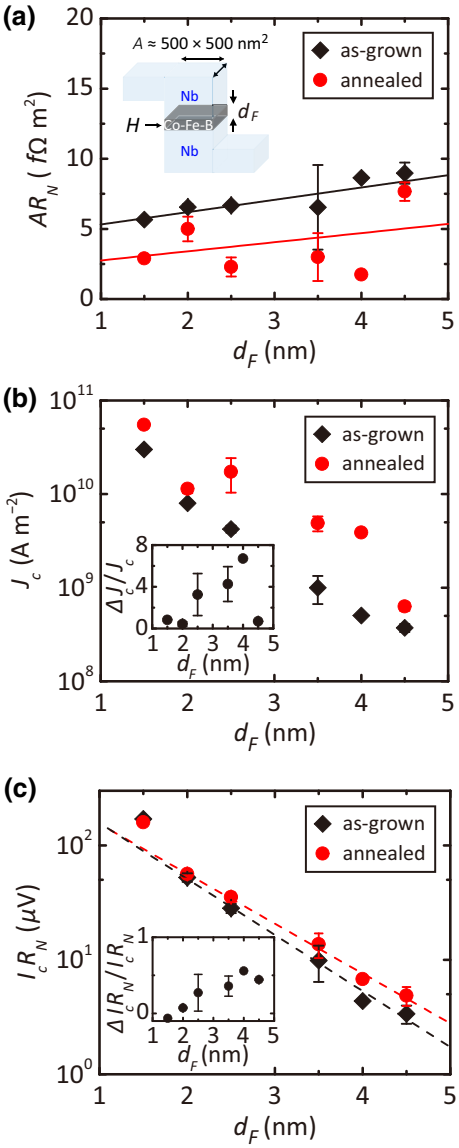

FIG. 2. (a) AR_N versus d_F before (black diamonds) and after (red circles) thermal annealing. The black line shows a least-squares regression-line fit for the nanopillars before annealing giving $\rho_F \approx (88 \pm 46)$ $\mu\Omega$ cm and $2AR_{\text{Nb/Co-Fe-B}} = (4.4 \pm 1.4)\, f\,\Omega$ m^2. For the annealed nanopillars, $\rho_F \approx (65 \pm 57)$ $\mu\Omega$ cm and $2AR_{\text{Nb/Co-Fe-B}} = (2.1 \pm 1.7)\, f\,\Omega$ m^2 from a least-squares regression-line fit (red line). (b) J_c versus d_F before (black diamonds) and after thermal annealing (red circles) at 400 °C for 30 min. The inset shows the relative change in J_c following thermal annealing $[(J_{c,\text{annealed}} - J_{c,\text{as-grown}})/J_{c,\text{as-grown}}]$ versus d_F. (c) I_cR_N versus d_F where the dashed lines are least-squares regression-line fits giving a coherence length in Co-Fe-B of $\xi_F = (0.93 \pm 0.02)$ nm and (1.00 ± 0.04) nm, for the nanopillars before and after thermal annealing, respectively. The inset shows the relative change in I_cR_N following thermal annealing $[(I_cR_{N,\text{annealed}} - I_cR_{N,\text{as-grown}})/I_cR_{N,\text{as-grown}}]$ versus d_F. The error bars in AR_N, J_c, and I_cR_N represent the statistical scatter for multiple nanopillars. All data at 1.6 K.

after annealing from a least-squares regression-line fit, implying that the interface resistance is approximately halved after annealing.

The decrease in R_N through thermal annealing results in a notable enhancement of J_c [Fig. 2(b)]. An enhancement of J_c is observed for all nanopillars investigated. The relative J_c change following thermal annealing [defined as $(J_{c,\text{annealed}} - J_{c,\text{as-grown}})/J_{c,\text{as-grown}}$] is 80–700% depending on the Co-Fe-B thickness [see inset of Fig. 2(b)]. Since J_c is inversely proportional to $AR_N = \rho_F \times d_F + 2AR_{\text{Nb/Co-Fe-B}}$, the influence of the relative ρ_F change on the relative J_c change should become larger with increasing d_F. However, the relative J_c change does not show a clear d_F dependence, implying that the relative J_c change is predominated by the variation in $R_{\text{Nb/Co-Fe-B}}$ induced by thermal annealing.

To investigate the effect of thermal annealing on the coherence length of superconductivity in Co-Fe-B, in Fig. 2(c) we plot the characteristic voltage (I_cR_N) versus d_F at 1.6 K before and after thermal annealing. In superconductor-ferromagnet-superconductor Josephson devices, I_cR_N typically oscillates with ferromagnetic barrier thickness due to 0–π phase transitions [23,31–35]. In our devices, I_cR_N exponentially decays with d_F but we do not observe 0–π oscillations, implying that the periodicity of the oscillations is either much shorter or longer than the d_F range investigated. From the Fermi velocity ($v_F = 1.1\times10^6$ m s^{-1} [30]) and the magnetic exchange energy of Co-Fe-B ($E_{\text{ex}} \approx k_B T_{\text{Curie}} = 113$ meV, where k_B is the Boltzmann constant and $T_{\text{Curie}} = 1313$ K [36]), an oscillation period is estimated to be $\pi v_F \hbar/2E_{\text{ex}}$ [37] ≈ 11 nm, which is much longer than the d_F range and hence undetectable in this study. However, we note that there is a recent study demonstrating a 0–π oscillation of period 0.5 nm in Nb/$Co_{56}Fe_{24}B_{20}$/Nb [10] and such a short periodicity could be the reason for the apparent absence of the oscillation in our nanopillars.

The inset of Fig. 2(c) shows the relative change of I_cR_N through thermal annealing [defined as $(I_cR_{N,\text{annealed}} - I_cR_{N,\text{as-grown}})/I_cR_{N,\text{as-grown}}$] increases with increasing d_F (i.e., the decay slope of I_cR_N with d_F becomes shallower as a result of annealing). By fitting the decay slope to $I_cR_N \propto \exp(-\xi_F/d_F)$, the coherence length of superconductivity in Co-Fe-B (ξ_F) is estimated to be (0.93 ± 0.02) nm and (1.00 ± 0.04) nm for the devices before and after annealing, respectively. Considering that the magnetic moment of Co-Fe-B is unchanged following thermal annealing [see Fig. 1(b)], the enhancement of ξ_F is likely due to an increase in the electron mean free path of Co-Fe-B as a result of improved structural ordering, consistent with the decrease in R_N in Fig. 2(a).

In conclusion, we demonstrate Josephson coupling through Co-Fe-B alloy and its optimization with thermal annealing in Nb/Co-Fe-B/Nb nanopillars. We find a notable enhancement of the Josephson critical current up to a maximum of 700% following thermal annealing at 400 °C, which is attributed to an increase in the proximity coherence length of superconductivity in Co-Fe-B and improved transparency at the Nb/Co-Fe-B interfaces. The thermal optimization of Josephson coupling following thermal annealing is attractive for the development of energy-efficient superconducting spintronic devices. Furthermore, electric current annealing treatments [38] on Josephson devices with Co-Fe-B could also tune device properties.

ACKNOWLEDGMENTS

We acknowledge funding from the EPSRC Programme Grant "Superspin" (No. EP/N017242/1) and the EPSRC International Network Grant "Oxide Superspin" (No. EP/P026311/1). J.E.T. acknowledges funding from DTP EPSRC Grants (No. EP/M508007/1 and No. EP/N509620/1).

[1] M. N. Baibich, J. M. Broto, A. Fert, F. N. Van Dau, F. Petroff, P. Eitenne, G. Creuzet, A. Friederich, and J. Chazelas, Giant Magnetoresistance of (001)Fe/(001)Cr Magnetic Superlattices, Phys. Rev. Lett. **61**, 2472 (1988).

[2] G. Binasch, P. Grünberg, F. Saurenbach, and W. Zinn, Enhanced magnetoresistance in layered magnetic structures with antiferromagnetic interlayer exchange, Phys. Rev. B **39**, 4828 (1989).

[3] B. Dieny, V. S. Speriosu, S. S. P. Parkin, B. A. Gurney, D. R. Wilhoit, and D. Mauri, Giant magnetoresistive in soft ferromagnetic multilayers, Phys. Rev. B **43**, 1297 (1991).

[4] B. Dieny, V. S. Speriosu, B. A. Gurney, S. S. P. Parkin, D. R. Wilhoit, K. P. Roche, S. Metin, D. T. Peterson, and S. Nadimi, Spin-valve effect in soft ferromagnetic sandwiches, J. Magn. Magn. Mater. **93**, 101 (1991).

[5] S. Tsunashima, M. Jimbo, Y. Imada, and K. Komiya, Spin valves using amorphous magnetic layers, J. Magn. Magn. Mater. **165**, 111 (1997).

[6] M. Jimbo, K. Komiyama, and S. Tsunashima, Giant magnetoresistance effect and electric conduction in amorphous-CoFeB/Cu/Co sandwiches, J. Appl. Phys. **79**, 6237 (1996).

[7] A. Sharma, M. A. Hoffmann, P. Matthes, O. Hellwig, C. Kowol, S. E. Schulz, D. R. T. Zahn, and G. Salvan, Crystallization of optically thick films of $Co_xFe_{80-x}B_{20}$: Evolution of optical, magneto-optical, and structural properties, Phys. Rev. B **101**, 054438 (2020).

[8] S. Ikeda, J. Hayakawa, Y. Ashizawa, Y. M. Lee, K. Miura, H. Hasegawa, M. Tsunoda, F. Matsukura, and H. Ohno, Tunnel magnetoresistance of 604% at 300 K by suppression of Ta diffusion in CoFeB/MgO/CoFeB pseudo-spin-valves annealed at high temperature, Appl. Phys. Lett. **93**, 082508 (2008).

[9] M. Jimbo, K. Komiyama, Y. Shirota, Y. Fujiwara, S. Tsunashima, and M. Matsuura, Thermal stability of spin valves using amorphous CoFeB, J. Magn. Magn. Mater. **165**, 308 (1997).

[10] M. G. Loving, T. F. Ambrose, S. Keebaugh, D. L. Miller, R. Pownall, N. D. Rizzo, A. N. Sidorov, and N. P. Siwak, Magnetic reversal and critical current transparency of CoFeB Superconductor-ferromagnet-superconductor heterostructures, ArXiv:2104.03188 (2021).

[11] S. U. Jen, Y. D. Yao, Y. T. Chen, J. M. Wu, C. C. Lee, T. L. Tsai, and Y. C. Chang, Magnetic and electrical properties of amorphous CoFeB films, J. Appl. Phys. **99**, 053701 (2006).

[12] V. V. Ryazanov, V. V. Bol, D. S. Sobanin, I. V. Vernik, K. Tolpygo, A. M. Kadin, and O. A. Mukhanov, Magnetic Josephson junction technology for digital and memory applications, Phys. Procedia **36**, 35 (2012).

[13] S. V. Bakurskiy, N. V. Klenov, I. I. Soloviev, V. V. Bol'ginov, V. V. Ryazanov, I. V. Vernik, A. Mukhanov, M. Y. Kupriyanov, and A. A. Golubov, Theoretical model of superconducting spintronic SIsFS devices, Appl. Phys. Lett. **102**, 192603 (2013).

[14] T. I. Larkin, V. V. Bol'ginov, V. S. Stolyarov, V. V. Ryazanov, I. V. Vernik, S. K. Tolpygo, and O. A. Mukhanov, Ferromagnetic Josephson switching device with high characteristic voltage ferromagnetic Josephson switching device with high characteristic voltage, Appl. Phys. Lett. **100**, 222601 (2012).

[15] C. Bell, G. Burnell, D.-J. Kang, R. H. Hadfield, M. J. Kappers, and M. G. Blamire, Fabrication of nanoscale heterostructure devices with a focused ion beam, Nanotechnology **14**, 630 (2003).

[16] A. I. Buzdin, Proximity effects in superconductor-ferromagnet heterostructures, Rev. Mod. Phys. **77**, 935 (2005).

[17] D. D. Djayaprawira, K. Tsunekawa, M. Nagai, H. Maehara, S. Yamagata, N. Watanabe, S. Yuasa, Y. Suzuki, and K. Ando, 230% room-temperature magnetoresistance in CoFeB/MgO/CoFeB magnetic tunnel junctions, Appl. Phys. Lett. **86**, 092502 (2005).

[18] S. X. Huang, T. Y. Chen, and C. L. Chien, Spin polarization of amorphous CoFeB determined by point-contact Andreev reflection, Appl. Phys. Lett. **92**, 242509 (2008).

[19] See Supplemental Material at http://link.aps.org/supplemental/10.1103/PhysRevApplied.17.L021002 for detailed electrical and magnetic properties of Nb/CoFeB/Nb nanopillars and CoFeB thin films.

[20] Y. M. Lee, J. Hayakawa, S. Ikeda, F. Matsukura, and H. Ohno, Effect of electrode composition on the tunnel magnetoresistance of pseudo-spin-valve magnetic tunnel junction with a MgO tunnel barrier, Appl. Phys. Lett. **90**, 2005 (2007).

[21] M. G. Blamire, C. B. Smiet, N. Banerjee, and J. W. A. Robinson, Field modulation of the critical current in magnetic Josephson junctions, Supercond. Sci. Technol. **26**, 055017 (2013).

[22] B. Börcsök, S. Komori, A. I. Buzdin, and J. W. A. Robinson, Fraunhofer patterns in magnetic Josephson junctions with non-uniform magnetic susceptibility, Sci. Rep. **9**, 5616 (2019).

[23] J. W. A. Robinson, S. Piano, G. Burnell, C. Bell, and M. G. Blamire, Zero to π transition in superconductor-ferromagnet-superconductor junctions, Phys. Rev. B **76**, 094522 (2007).

[24] E. Nazaretski, J. P. Thibodaux, I. Vekhter, L. Civale, J. D. Thompson, and R. Movshovich, Direct measurements of the penetration depth in a superconducting film using magnetic force microscopy, Appl. Phys. Lett. **95**, 262502 (2009).

[25] S. Komori, J. M. Devine-stoneman, K. Ohnishi, G. Yang, Z. Devizorova, S. Mironov, X. Montiel, L. A. B. O. Olthof, L. F. Cohen, H. Kurebayashi, M. G. Blamire, A. I. Buzdin, and J. W. A. Robinson, Spin-orbit coupling suppression and singlet-state blocking of spin-triplet Cooper pairs, Sci. Adv. **7**, eabe0128 (2021).

[26] N. Heiman, R. D. Hempsted, and N. Kazama, Low-coercivity amorphous magnetic alloy films, J. Appl. Phys. **49**, 5663 (1978).

[27] A. Buzdin, Peculiar properties of the Josephson junction at the transition from 0 to π state, Phys. Rev. B **72**, 100501(R) (2005).

[28] H. Sellier, C. Baraduc, and R. Calemczuk, Half-Integer Shapiro Steps at the 0–π Crossover of a Ferromagnetic Josephson Junction, Phys. Rev. Lett. **92**, 257005 (2004).

[29] J. Kim, J. H. Kwon, and K. Char, Quantitative analysis of the proximity effect in Nb/$Co_{60}Fe_{40}$, Nb/Ni, and Nb/$Cu_{40}Ni_{60}$ bilayers, Phys. Rev. B **72**, 014518 (2005).

[30] A. Useinov, O. Mryasov, and J. Kosel, Output voltage calculations in double barrier magnetic tunnel junctions with asymmetric voltage behavior, J. Magn. Magn. Mater. **324**, 2844 (2012).

[31] A. I. Buzdin, L. N. Bulaevskii, and S. V. Panyukov, Critical-current oscillations as a function of the exchange field and thickness of the ferromagnetic metal (F) in an S-F-S Josephson junction, JETP Lett. **35**, 178 (1982).

[32] A. I. Buzdin and M. Y. Kupriyanov, Transition temperature of a superconductor-ferromagnet superlattice, JETP Lett. **52**, 487 (1990).

[33] H. Sellier, C. Baraduc, F. Lefloch, and R. Calemczuk, Temperature-induced crossover between 0 and π states in S/F/S junctions, Phys. Rev. B **68**, 054531 (2003).

[34] T. Kontos, M. Aprili, J. Lesueur, F. Genêt, B. Stephanidis, and R. Boursier, Josephson Junction Through a Thin Ferromagnetic Layer: Negative Coupling, Phys. Rev. Lett. **89**, 137007 (2002).

[35] Y. Blum, A. Tsukernik, M. Karpovski, and A. Palevski, Oscillations of the Superconducting Critical Current in Nb-Cu-Ni-Cu-Nb Junctions, Phys. Rev. Lett. **89**, 187004 (2002).

[36] K. Nagasaka, L. Varga, Y. Shimizu, S. Eguchi, and A. Tanaka, The temperature dependence of exchange anisotropy in ferromagnetic/PdPtMn bilayers, J. Appl. Phys. **87**, 6433 (2000).

[37] J. W. A. Robinson, S. Piano, G. Burnell, C. Bell, and M. G. Blamire, Critical Current Oscillations in Strong Ferromagnetic Junctions, Phys. Rev. Lett. **97**, 177003 (2006).

[38] S. Collienne, B. Raes, W. Keijers, J. Linek, D. Koelle, R. Kleiner, R. B. G. Kramer, J. Van De Vondel, and A. V. Silhanek, Nb-Based Nanoscale Superconducting Quantum Interference Devices Tuned by Electroannealing, Phys. Rev. Appl. **15**, 1 (2021).